Midnight radial profiles of the quiet and growth-phase plasma sheet: The Geotail observations

Chih-Ping Wang and Larry R. Lyons
Department of Atmospheric and Oceanic Sciences, University of California, Los Angeles, California, USA

T. Nagai
Department of Earth and Planetary Sciences, Tokyo Institute of Technology, Tokyo, Japan

J. C. Samson
Department of Physics, University of Alberta, Edmonton, Alberta, Canada

Received 18 May 2004; accepted 25 August 2004; published 2 December 2004.

[1] To evaluate the plasma sheet transition from weak to strong convection, we investigate ion moments and magnetic field observed by Geotail. The Geotail data from 1995 to 1997 within the area $-9\ R_E \geq X_{\mathrm{GSM}} \geq -30\ R_E$ and $|Y_{\mathrm{GSM}}| \leq 5\ R_E$ were sorted for periods of quiet times and the substorm growth phase, which gives a better indication of convection strength than do global indexes. We find that the overall growth-phase ion pressure is a factor of ~1.55 higher than the quiet-time ion pressure. Density is higher and temperature is lower during quiet times. Ions drift mainly earthward and duskward, and the drift speed is about twice stronger during the growth phase. The duskward drift is dominated by ions' diamagnetic drift. The $|B_x|$ in the lobes increases strongly, while B_z near the current sheet at small radial distance decreases as convection increases, indicating that field lines become more stretched during the growth phase because of the earthward penetration of the plasma sheet. The increase in the lobe magnetic field is sufficient to maintain force balance in the z direction with the enhanced ion pressure in the plasma sheet. Intervals of negative B_z are observed during both quiet and growth-phase conditions. The observed negative B_z intervals near the current sheet are short and are likely caused by perturbations, while those in the lobes are substantially longer and are likely associated with field line flaring. *INDEX TERMS:* 2764 Magnetospheric Physics: Plasma sheet; 2760 Magnetospheric Physics: Plasma convection; 2740 Magnetospheric Physics: Magnetospheric configuration and dynamics; 2744 Magnetospheric Physics: Magnetotail; 2731 Magnetospheric Physics: Magnetosphere—outer; *KEYWORDS:* plasma sheet, Geotail, quiet time, substorm growth phase, ion moments, magnetic field

Citation: Wang, C.-P., L. R. Lyons, T. Nagai, and J. C. Samson (2004), Midnight radial profiles of the quiet and growth-phase plasma sheet: The Geotail observations, *J. Geophys. Res.*, *109*, A12201, doi:10.1029/2004JA010590.

1. Introduction

[2] The spatial and time variations of plasma moments and magnetic field in the plasma sheet are crucial to geomagnetic disturbances. Plasma transport and energization driven by convection in the Earth's magnetosphere is believed to play a major role in causing these variations, but there is a theoretical argument that questions whether stability of the plasma sheet can be maintained when magnetosphere convection is enhanced [*Erickson and Wolf*, 1980]. Therefore the radial profiles along the midnight meridian, along which energization is expected to be the most significant as plasma drift earthward from the tail, provide important information in understanding how convection results in plasma sheet formation.

0148-0227/04/2004JA010590$09.00

[3] The pressure in the plasma sheet is reported to increase with decreasing distance from the Earth for all levels of activity [*Angelopoulos et al.*, 1993; *Angelopoulos*, 1996; *Huang and Frank*, 1986, 1994b] and to be stronger during disturbed times [*Spence et al.*, 1989; *Kistler et al.*, 1992, 1993; *Nagai et al.*, 1997]. No strong dependence of the equatorial magnetic field strength in the plasma sheet has been found with radial distance [*Huang and Frank*, 1994a; *Nakamura et al.*, 1994] and with activity level [*Huang and Frank*, 1994a]. However, the magnetic field configuration becomes more tail-like during higher activity [*Fairfield et al.*, 1987; *Kistler et al.*, 1993]. The pressures in the lobes and plasma sheet can balance each other for different levels of activity [*Fairfield et al.*, 1981; *Baumjohann et al.*, 1990]. However, most of the previous studies evaluated the plasma sheet corresponding to different levels of geomagnetic activity by using a global index such as Kp and AE. Since activity can be high while

convection is weak, such as that happens during the substorm expansion and recovery phases, the previous results may not able to clearly show plasma sheet differences under different strengths of convection.

[4] Our goal in this study is to investigate the difference in the plasma sheet when driven by weak and by strong convection. Even though solar wind data are the best to indicate convection strength, we avoid using it here because of the uncertainty in determining when and if the observed IMF structure really hits the Earth's magnetosphere. It is well accepted that convection is weakest when the magnetosphere is quiet and that convection is enhanced during the substorm growth phase. Large temporal variations in magnetic field and intense aurora are not seen during these two periods, which indicates the magnetosphere is relatively stable and that convection is likely the dominated process in the plasma sheet. Thus observations during these two different conditions should reveal the general plasma sheet structure under weak and strong convection.

2. Instrumentation and Data

[5] We have obtained data from the Geotail spacecraft from the DARTS/GEOTAIL website. We used the 12 s resolution ion data obtained by the low-energy particle (LEP) instrument [*Mukai et al.*, 1994] over the energy range from 31 eV/q to 39 keV/q, and 3 s magnetic field data from the magnetic field (MGF) experiment [*Kokubun et al.*, 1994]. The moments and magnetic field data in GSM coordinate are used. Data from 1995 to 1997 and in the area $|Y_{GSM}| \leq 5\ R_E$ and $0 \geq X_{GSM} \geq -30\ R_E$ are used in this study.

[6] AE and PCNorth index (Polar Cap Magnetic Activity index), together with the data from auroral magnetometer chains including Greenland, CANOPUS, Alaska, and IMAGE, the magnetometer data from three stations in Russia (Tixie, Kotel'nyy, and Chokurdakh), and energetic electron and ion fluxes at geosynchronous orbit satellites were used to determine periods of quiet times and of substorm growth phase. The quiet periods were chosen to have AE $\leq$ 50 nT and PCNorth $\leq$ 0.5 and no large disturbance in the ground magnetometer data and the geosynchronous particle fluxes. Substorms were identified by signatures such as dipolarization seen by Geotail, strong decrease in the H component of magnetic field observed by the ground magnetometer stations listed above when they are near the local midnight (Pi 2 activity was investigated only in the CANOPUS data), and electron or ion injection detected by geosynchronous satellites. The onset time of the expansion phase or pseudo-breakup was determined by the ground signatures and particle injections (Geotail depolarization is not always clear, especially when Geotail is beyond $X_{GSM} \sim -20\ R_E$). We exclude substorm events with no particle injection observed by the geosynchronous orbit satellites, thus including only substorms that happened following stronger convection and helping to clarify the difference from the quiet-time plasma sheet. Substorms that occurred during the recovery phase of a proceeding substorm are also not included. Growth-phase data within the period 30 min prior to the onset of the expansion phase were used. There are 130 30 min growth-phase periods and 333 30 min quiet periods used in this study. Figure 1 gives the positions of Geotail during the chosen quiet and growth-phase periods and shows that there is reasonably uniform coverage of the area $|Y_{GSM}| \leq 5\ R_E$ and $0 \geq X_{GSM} \geq -30\ R_E$ plane for both periods.

[7] Data for each type of period were then separated into two regions according to the ratio of plasma pressure (P_{ion}) to magnetic pressure ($P_{mag} = B^2/(2\mu_0)$). We identify Geotail as being in the central plasma sheet (CPS) if $P_{ion} \geq 3P_{mag}$ and in the lobes if $P_{mag} \geq 3P_{ion}$. Data points for $3P_{mag} > P_{ion} > P_{mag}/3$ were not used unless otherwise indicated.

3. Results and Analysis

3.1. Ion Pressure

[8] During quiet times and the growth phase, the pressure from ions whose energy higher than the LEP upper energy cutoff (39 keV/q) is usually very small so the LEP pressure represents well the total ion pressure. In a few of our growth-phase events, the peak of particle fluxes is near the LEP highest-energy channel but our investigations of these events show that the LEP ion pressure still represents $\sim$90 % of total ion pressure. The ion pressures in the CPS and the total pressure (ion pressure plus magnetic pressure) in the lobes for quiet times and the growth phase are shown in Figure 2, together with pressures averaged over an area of 2.5 R_E in the x direction and 10 R_E in the y direction ($|Y_{GSM}| \leq 5\ R_E$). The same process to obtain the spatial average of pressure is also used for all other moments and magnetic field data shown in this paper except perpendicular drift velocity. We find that pressures for both periods increase with decreasing distance from the Earth, as reported previously [e.g., *Spence et al.*, 1989; *Angelopoulos et al.*, 1993]. We also find that there is a clear pressure difference between the two periods, with higher pressures during the growth phase at all radial distance. The higher growth-phase plasma pressure is also reported by *Kistler et al.* [1992, 1993] and *Nagai et al.* [1997]. The overall ion (total) pressure throughout the plasma sheet during the growth phase is a factor of $\sim$1.55 (1.75) higher than that during the quiet times.

[9] The average Geotail ion pressure profile for quiet times in Figure 2c is almost the same as the AMPTE quiet-time ion pressure reported by *Angelopoulos et al.* [1993] but is a factor of $\sim$1.5–2 higher than the ISEE 2 ion pressure measured for Kp = 1^- [*Spence et al.*, 1989]. For the growth phase, the Geotail total pressure shown in Figure 2f is only slightly lower than the AMPTE total pressure measured during the substorm growth phase inside $|Y_{GSM}| = 15\ R_E$ [*Kistler et al.*, 1993]. However, the Geotail growth-phase ion pressure shown in Figure 2c is almost a factor of 2 higher than the ISEE 2 ion pressure measured for Kp = 3^-. The lower pressure observed by ISEE 2 is likely due to the less strict plasma sheet criteria used. That the ISEE 2 pressure sorted for Kp = 3^- may include periods of substorm expansion and recovery phase, during which the magnetosphere is disturbed but convection may be weak, can also contribute to their lower pressure. These comparisons with the two separate studies of the AMTPE data indicate that our data set does indeed describe the plasma sheet during weak and strong convection.

[10] Figure 3 compares the average total pressures in the CPS and lobes. For quiet times, we can see in Figure 3a the

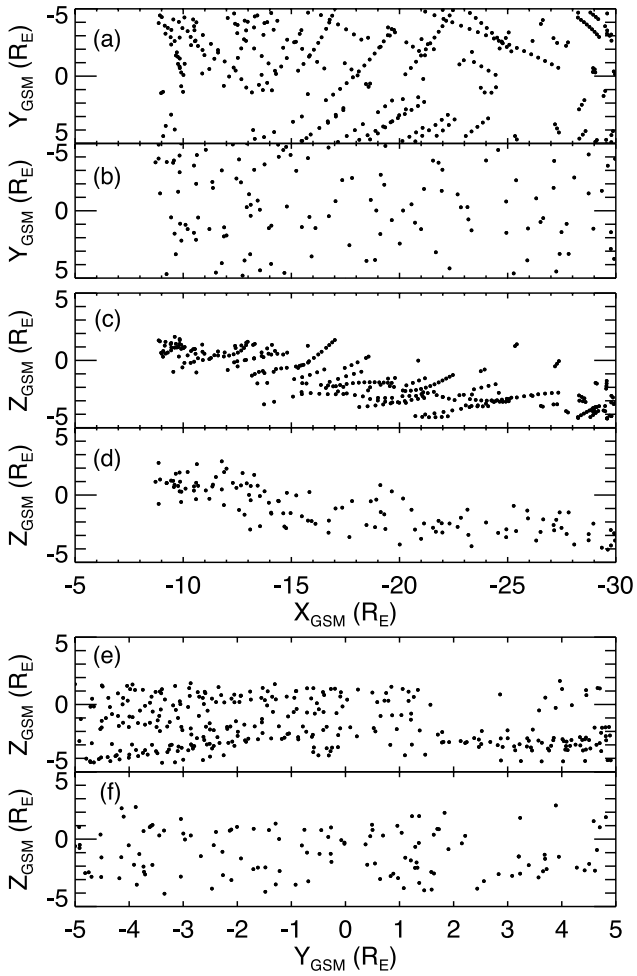

Figure 1. Geotail positions for quiet times in the (a) *x-y* plane, the (c) *x-z* plane, and the (e) *y-z* plane. Geotail positions for the substorm growth phase in the (b) *x-y* plane, the (d) *x-z* plane, and the (f) *y-z* plane.

total pressures in the CPS and lobes are roughly the same. However, during the growth phase as shown in Figure 3b, the total pressures in the lobes become clearly higher than those in CPS at $X_{GSM} \geq -13\ R_E$. However, this difference does not imply pressure imbalance in the *z* direction and is expected from the general increase in total pressure and thinning of the plasma sheet that occur during the growth phase. In Figure 4 we averaged total pressure (all data points are used) for every 5 min within each 30 min interval ($t = 0$ is the start of the 30 min period), and normalize each averaged total pressures to the average total pressure at the last 5 min (which is just before the expansion onset for the growth phase). It can be seen that during the 30 min period the total pressure increases during the growth phase and the increase is more significant at smaller radial distance. The pressure increase during the growth phase was also reported by *Nagai et al.* [1997]. However, the total pressure remains constant for the quiet times, when persistent pressure change is not expected. On the other hand, because of the plasma sheet thinning, the Geotail location is likely to change from the CPS to the lobes during the 30 min period. As we will discuss in 3.4, magnetic field line stretching that results in plasma sheet thinning is more prominent in the near Earth plasma sheet. Therefore the higher growth-phase lobe total pressure seen in the near Earth plasma sheet in Figure 3b results from the spacecraft being more likely to be within the lobes near the end of the growth phase when pressures are highest.

3.2. Ion Density and Temperature

[11] Figure 5 shows the number density in the CPS for the two types of periods. It can be seen that most of the density measurements during quiet times were higher than those measured during the growth phase. Figure 5c shows that the average densities during quiet conditions are about a factor of 1.45 higher than the densities during growth-phase conditions. It has been shown that the low-latitude boundary layer (LLBL) can supply cold particles into the plasma sheet much more efficiently during northward IMF than during southward IMF [*Terasawa et al.*, 1997; *Fujimoto et al.*, 1998], suggesting the quiet-time plasma sheet is a mixture of plasma from the mantle and colder and denser plasma from the LLBL.

[12] To investigate whether the contribution of the LLBL particles can account for the higher quiet-time total number density, we plot in Figure 6 the number densities for measurements with temperature higher or lower than

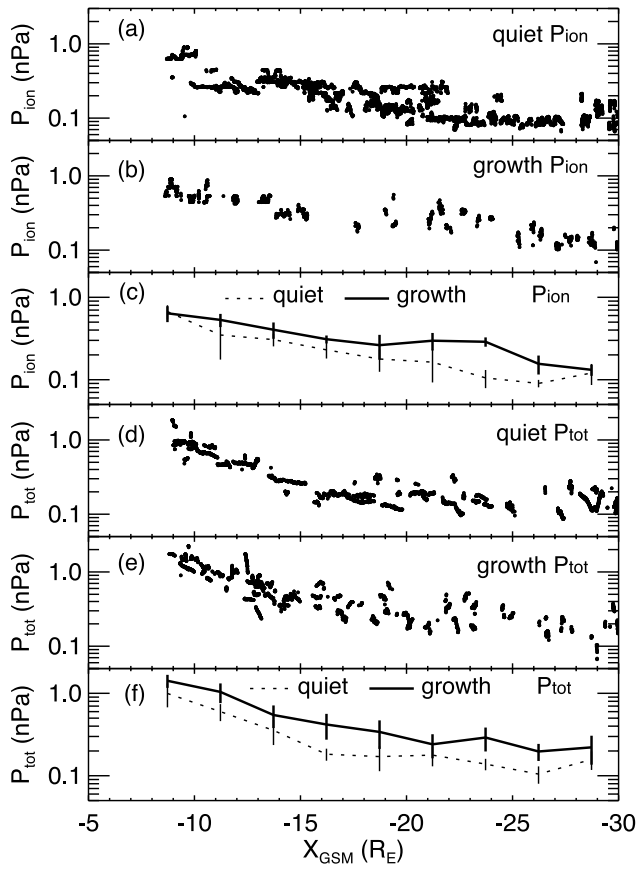

Figure 2. Radial profiles of the ion pressure in the CPS for (a) quiet times, (b) the growth phase, and (c) the comparisons of the averaged pressures (the vertical lines indicate the standard deviations). Radial profiles of the total pressure in the lobes for (d) quiet times, (e) the growth phase, and (f) the averaged pressures.

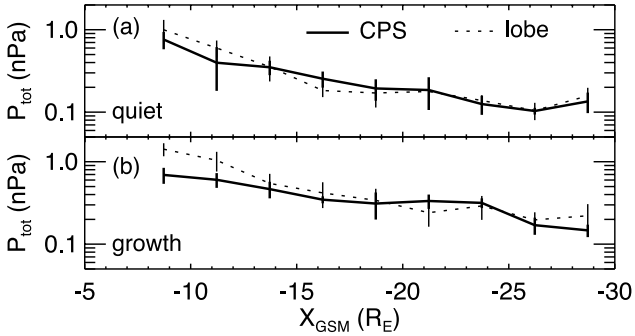

Figure 3. Comparisons between the averaged total pressures in the CPS and lobes for (a) quiet times and for (b) the growth phase.

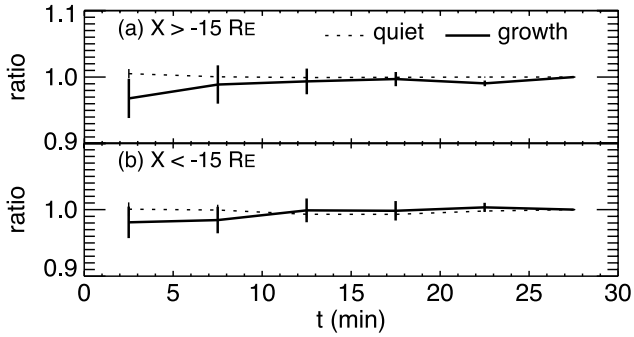

Figure 4. Comparisons between the time variations of the total pressures normalized by the total pressure at the end of each 30 min period for quiet times and the growth phase in the region (a) $X_{GSM} > -15\ R_E$ and (b) $X_{GSM} < -15\ R_E$.

3 keV (the 3 keV is an arbitrary criteria and a more realistic energy discriminator would decrease with increasing X, however we do not have a clear idea as to what would be a realistic variation to chose). This figure clearly shows that the plasma number density is substantially higher when the temperature is low than when it is high, and that such high-density, low-temperature plasma is far more common during quiet times than during disturbed times. This indicates that the LLBL particles can drift from the tail flanks into the midnight plasma sheet during quiet times and have significant contribution. However, there are many measurements during quiet times with lower density and higher temperature, which implies that the access of the LLBL particles to the plasma sheet or the LLBL itself may have spatial and time variation during quiet times. It is also possible that cases without significant LLBL contribution occur around the beginning of quiet periods, before the slow moving LLBL ions from the flank have had time to drift to the midnight region. That the LLBL contribution to the plasma sheet becomes much less during the growth phase is consistent with previous studies [*Terasawa et al.*, 1997; *Fujimoto et al.*, 1998].

[13] Figures 6a and 6c shows that when there is little LLBL contribution, the number density increases with decreasing distance from the Earth and, as shown by the averages in Figure 6e, is perhaps slightly higher during the growth phase. The number density with strong LLBL contribution, as shown in Figures 6b and 6d, also increases with decreasing distance from the Earth.

[14] Because of the mixing of cooler ions from the LLBL with warmer ions from the mantle, ion temperature is therefore not a clear indication of the thermal energy of a single population, but instead indicates how significant the contribution of the LLBL is. As shown in Figure 7, there are much more low-temperature measurements during quiet periods and, as a result, the averaged quiet-time temperature is a factor of $\sim$2 lower than the growth-phase temperature. Figure 7 also shows the highest temperature observed during the growth phase is higher than those observed during quiet times, especially at smaller radial distance, which suggests that the quiet-time temperature may be still somewhat lower than the growth-phase temperature even without the LLBL contribution. Figure 7d shows that when we exclude data with temperature lower than 3 keV the quiet-time temperature becomes only slightly lower than the growth-phase temperature. However, the quiet-time temperature with the <3 keV points excluded is nearly independent of X, which is probably the result of our using an X-independent energy discriminator.

3.3. Perpendicular Velocity

[15] The drift in the plasma sheet is often observed to oscillate in magnitude with a period of several minutes for both quiet and growth condition. The drift direction oscillates as well because the amplitude of the oscillation is often comparable to or bigger than the average drift speed. This is likely a result of drift caused by plasma oscillations, such as Pc5, on top of large- scale electric and magnetic drift.

[16] Owing to nonuniform efficiency among the seven Geotail ion detectors looking at different elevation angles, there is an offset of $\sim$7 km/s in the GSM V_z [*Katamura*, 1997]. We have checked our data set following *Katamura*'s [1997] analysis and found that the offset differs at different radial distance with a range from 5 km/s to 15 km/s. Therefore we subtracted V_z from the radial distance–dependent offsets before we calculated the perpendicular drift velocity V_{perp}. Note that the offset we subtracted from V_z can introduce uncertainty to V_{perp}. Figure 8 shows the radial profiles of perpendicular velocity in the x-y plane for Y_{GSM} >

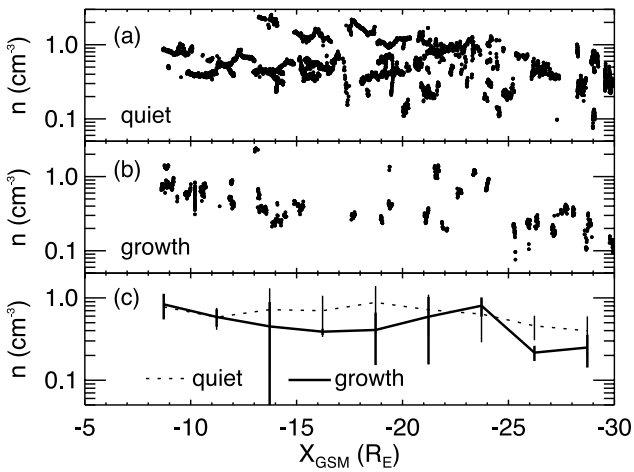

Figure 5. Ion number density in the CPS for (a) quiet times, (b) the growth phase, and (c) the comparisons of the averaged densities.

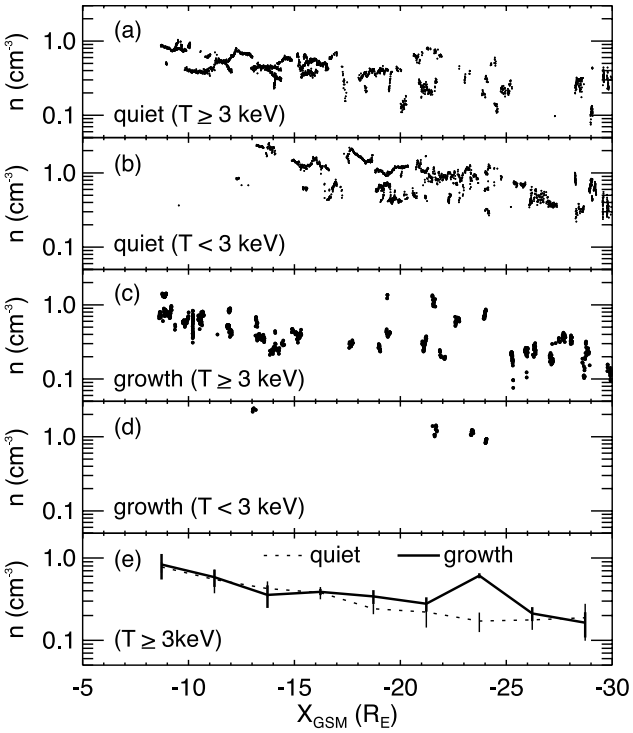

Figure 6. Ion number density in the CPS for quiet times with temperature (a) >3 keV and (b) <3 keV. Ion number density in the CPS during the growth phase with temperature (c) >3 keV and (d) <3 keV. Averaged number densities for data with temperature (e) >3 keV.

0 and $Y_{GSM} < 0$ and the velocities averaged over an area of 5 R_E in the x direction and 5 R_E in the y direction. The amplitudes of the oscillations in drifts are bigger than the average drifts. The oscillations are stronger at larger radial distance but the average drifts decreases with increasing radial distance. During quiet times in the $Y_{GSM} < 0$ region $V_{perp,x}$ is nearly zero and $V_{perp,y}$ is ~20 km/s at small radial distance but decreases quickly with increasing radial distance. In the $Y_{GSM} > 0$ region the drift is stronger with $V_{perp,x}$ ~5 km/s and $V_{perp,y}$ ~20 km/s and $V_{perp,y}$ is less dependent on radial distance than it is in the $Y_{GSM} < 0$ region. During the growth phase there is no significant increase in the drift in the $Y_{GSM} < 0$ region, however in the $Y_{GSM} > 0$ region inside $X_{GSM} = -20$ R_E $V_{perp,x}$ increases strongly to ~25 km/s and $V_{perp,y}$ to ~60 km/s. The flow speed averaged throughout the plasma sheet increases by a factor of ~2 from quiet to growth condition. Higher flow speed during higher activity was also reported by *Zhu* [1993].

[17] That the quiet-time flow is dominated by duskward drift as shown in Figure 8 is also seen in the quiet-time flows observed by AMPTE and ISEE [*Angelopoulos et al.*, 1993] but the flow speed measured by AMPTE and ISEE (~50 km/s) is higher than the Geotail flow speed. The Geotail flow averaged over all levels of activity reported by *Hori et al.* [2000] shows stronger earthward flow than our quiet-time and growth-phase flow. In addition to the different criteria used in these studies to identify the region of the plasma sheet, the difference in speed is likely a result that we used perpendicular drift velocity while *Angelopoulos et al.* [1993] and *Hori et al.* [2000] used total drift, which can be affected by drift in the parallel direction especially when a spacecraft is near the plasma sheet boundary layer.

[18] We expect the $V_{perp,x}$ shown in Figure 8 would underestimate the perpendicular drift speed at the center of current sheet where $B_x = 0$ since $V_{perp,x}$ decreases as the elevation angle ($\tan^{-1}(B_z/B_x)$) of magnetic field becomes smaller and the $V_{perp,x}$ shown in Figure 8 is an average of data that include measurements at small elevation angles, During the growth phase, the drift due to induction electric field resulting from field line stretching, which is in the opposite direction to the earthward convection electric drift, becomes important. Therefore in addition to the elevation effect, we expect that the $V_{perp,x}$ observed by Geotail, which includes both induction and convection electric drift, would underestimate the earthward convection speed during the growth phase. Since the magnetic field lines around midnight are mainly along the x-z plane, the above effects do not strongly affect $V_{perp,y}$.

[19] The duskward drift can be explained by the direction of ion diamagnetic drift, $\mathbf{B} \times \nabla p/(neB^2)$, where ∇p, as shown in Figure 2, is pointed toward the positive x direction. The estimated magnitude of ion's diamagnetic drift using the averaged values shown in Figures 2, 5, and 9 is in the same order of magnitude as the observed average drift shown in Figure 8.

3.4. Magnetic Field

[20] As shown in Figure 9, the quiet-time $|B_x|$ in the CPS gradually increases with decreasing radial distance from the Earth. However, the quiet-time B_z in the CPS, and also $|B_x|$ and B_z in the lobes, remains almost constant as the radial distance decreases from -30 R_E to approximately -15 R_E but quickly increases inside -15 R_E. The sharp change in the radial gradient indicates the transition from tail-like field

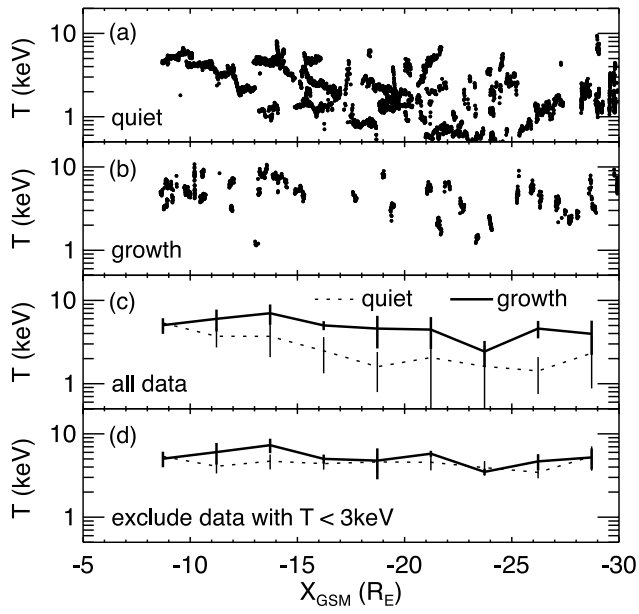

Figure 7. Ion temperature in the CPS for (a) quiet times, (b) the growth phase, and the comparisons of the averaged temperatures (c) including all data and (d) excluding data with temperature lower than 3 keV.

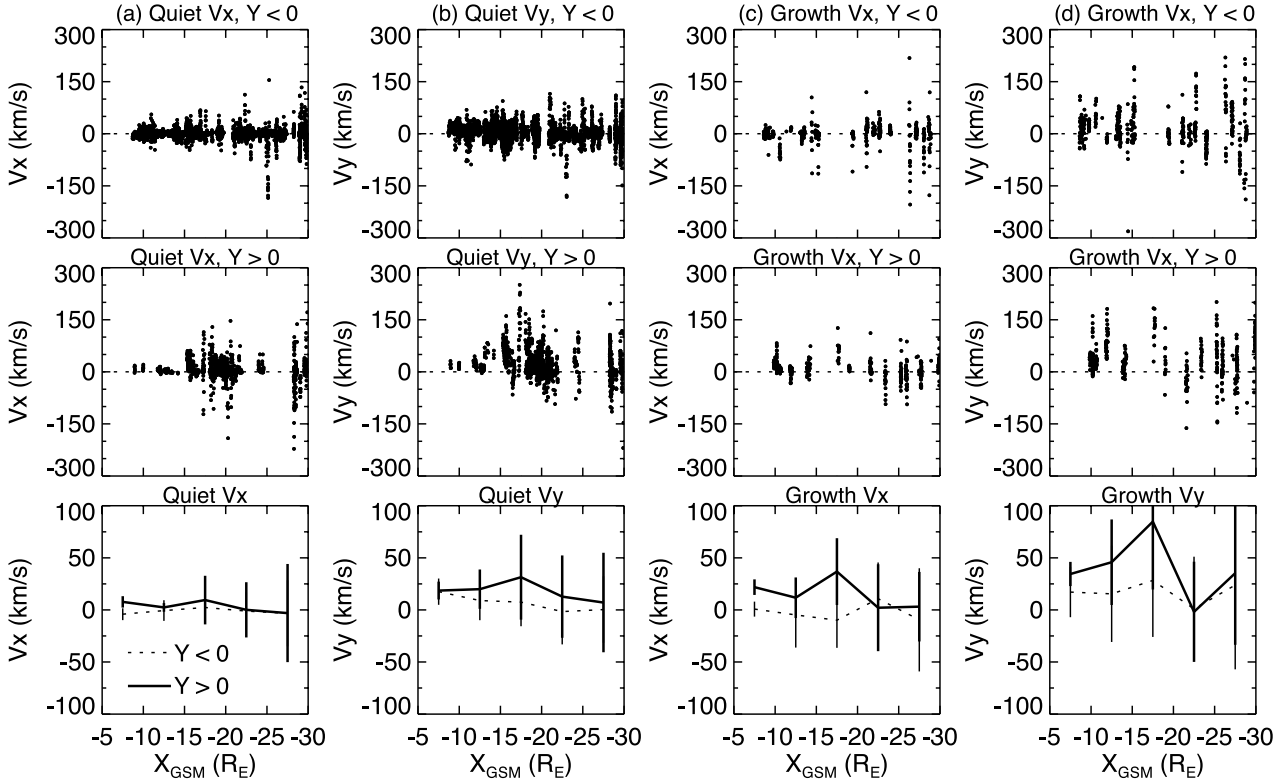

Figure 8. Quiet-time perpendicular ion drift (a) V_x and (b) V_y and the growth phase perpendicular ion drift (c) V_x and (d) V_y for the region of (top) $Y_{GSM} \leq 0$, (middle) $Y_{GSM} \geq 0$, and (bottom) comparisons between the average velocity for $Y_{GSM} \leq 0$ and $Y_{GSM} \geq 0$.

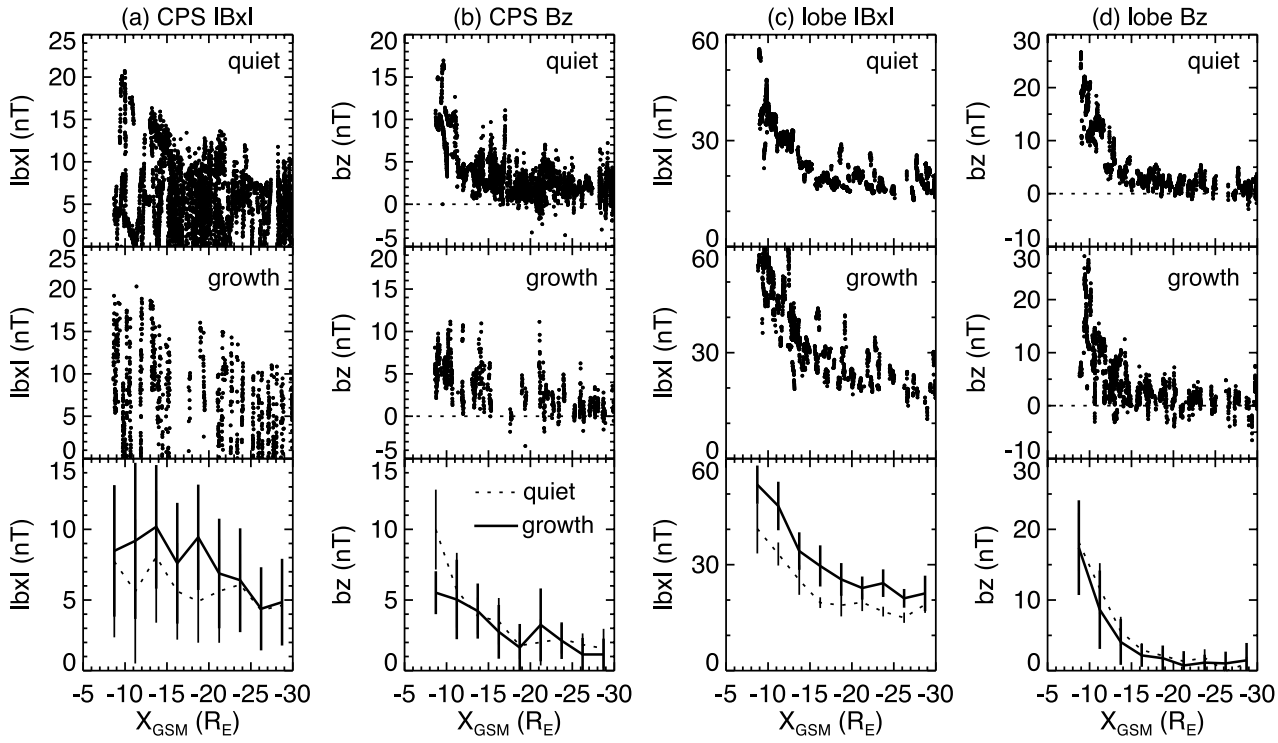

Figure 9. (a) $|B_x|$ in the CPS, (b) B_z in the CPS, (c) $|B_x|$ in the lobes, and (d) B_z in the lobes for (top) quiet times, (middle) the growth phase, and (bottom) the averaged fields.

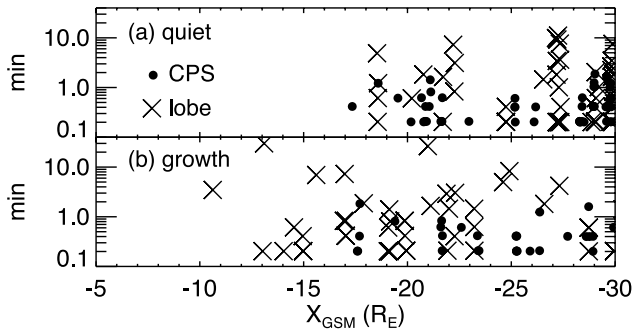

Figure 10. Durations of B_z remaining negative during (a) quiet times and (b) the growth phase.

in the plasma sheet to dipole-like field in the inner magnetosphere. In the CPS during quiet times, $|B_x|$ is about twice $|B_z|$ beyond -15 R_E but becomes smaller than $|B_z|$ at smaller radial distance. In the lobes $|B_x|$ dominates at all X, being a factor of 2–3 stronger than $|B_z|$.

[21] During the growth phase $|B_x|$ increases slightly in the CPS. B_z remains the same tailward of -12 R_E but decreases earthward of -12 R_E, therefore the radial profile becomes flatter. In the lobes $|B_x|$ increases at all radial distance, the increase being larger at smaller radial distance, while B_z decreases slightly inside -20 R_E. These changes clearly indicate that the field lines in both the CPS and lobes become more stretched during the growth phase. The reduction in B_z inside -12 R_E reflects the earthward penetration of the plasma sheet, and thus of the transition between tail-like and dipole-like field lines, that occurs during the growth phase.

[22] The average increase in the lobe magnetic field strength throughout the plasma sheet is about a factor of 1.34, giving a magnetic energy density increase of 1.8, which is comparable to the increase factor of 1.55 in the CPS ion pressure. This indicates the pressure balance between the CPS and lobes is maintained in the z direction as convection increases. This is consistent with previous results [*Fairfield et al.*, 1981; *Baumjohann et al.*, 1990].

[23] Figure 9 also shows that B_x is significant larger in the lobes than in the CPS at all X during both quiet and growth periods as expected. However, B_z in the CPS is roughly the same as that in the lobes beyond -12 R_E and is smaller inside -12 R_E. This is contrary to the ISEE observations reported by *Huang and Frank* [1994a, 1994b], which show B_z decreases significantly in the z direction away from the current sheet.

[24] As shown in Figure 9, instances of negative B_z are observed at larger radial distances in both the CPS and lobes and for both quiet and growth periods, and negative B_z in the lobes appears more often and is larger during the growth phase. Figure 10 shows the time duration of intervals of negative B_z. We find that longer intervals of continuously negative B_z are observed in the lobes than in the CPS, as reported before [*Fairfield*, 1986; *Nakamura et al.*, 1994]. We also see that negative B_z is not observed inside $X_{GSM} = -17$ R_E during quiet times in both the CPS and lobes. There is little difference in the distribution of negative B_z in the CPS between growth-phase and quiet periods, but negative B_z within the lobes is observed as close as $X_{GSM} = -11$ R_E during the growth phase. In the CPS, all the negative B_z intervals lasted for less than 2 min regardless of convection strength, which suggests that they are transient phenomena and are probably caused by perturbations whose amplitudes becoming comparable with the weak background field at large radial distance. On the other hand, the negative B_z in the lobes lasts much longer and is thus probably associated with large-scale flaring of field lines at higher Z. During strong convection, the field lines at smaller radial distance become more stretched and the flaring region likely extends to the lower Z range of Geotail's positions, so that negative B_z can be observed.

4. Summary

[25] We have investigated the plasma moments and magnetic field data measured by Geotail near the midnight meridian during periods of quiet times (weak convection) and the substorm growth phase (strong convection) in order to evaluate the dependence of the plasma sheet on convection strength. Using data during the growth phase to represent the plasma sheet under strong convection avoids processes, such as dipolarizations, that could also affect the large-scale plasma sheet.

[26] The total pressure in the plasma sheet generally remains constant during a 30 min quiet-time period but generally increases during a 30 min growth-phase period. For both weak and strong convection, the pressure increases with decreasing distance from the Earth. On the average, we find the overall ion pressure within the CPS (the total pressure within the lobes) to be a factor of ~1.55 (1.75) higher during the growth phase than during quiet times. Since our averages are over 30 min periods prior to substorm onsets, and pressure typically increases during this 30 min period, the peak pressure increases would be somewhat stronger than the above averages.

[27] The number density and temperature of the plasma sheet are strongly affected by cold particles drifting from the LLBL during quiet times, whereas the LLBL contribution decreases significantly under strong convection. This results in the plasma sheet being significantly denser and colder during quiet times than during periods of enhanced convection.

[28] The perpendicular ion drift consists of large-scale electric and magnetic drifts and perturbations with periods of several minutes and amplitudes comparable to or bigger than the averaged drift. The averaged drift is dominated by earthward and duskward flow and overall drift speed during the growth phase is a factor of ~2 larger than the quiet-time drift speed. The duskward drift is expected to be dominated by diamagnetic drift, which results from the ion's earthward radial pressure gradient.

[29] The magnetic field changes more significantly at smaller radial distance as convection becomes stronger. From quiet times to the growth phase, B_z in both the CPS and lobes goes down while B_x increases more strongly in the lobes than in the CPS, indicating that field lines become more stretched during strong convection as a result of the earthward penetration of the plasma sheet. The overall increase in the lobe magnetic field is sufficient to balance the increase of ion pressure in the CPS and to thus maintain magnetosphere stability in the z direction. Negative B_z is

observed at larger radial distance. It is transient in the CPS but can lasts much longer in the lobes. The negative B_z in the lobes, but not in the CPS, can be seen at smaller distance when convection is strong. The negative B_z in the CPS is likely caused by perturbations while that in the lobes is likely associated with high-latitude field line flaring.

[30] In a companion paper [*Wang et al.*, 2004], we will compare the observations presented in this paper with the simulation results from our plasma sheet model to investigate if the adiabatic drift transport and energization associated with electric and magnetic drift can quantitatively account for the observed plasma sheet transition from weak to strong convection.

[31] **Acknowledgments.** This work has been supported at UCLA by NSF grant ATM- 0207298. Research support for J. C. Samson was in part by the Natural Sciences and Engineering Research Council of Canada. Geotail magnetic field data were provided by S. Kokubun and plasma data by T. Mukai through DARTS at the Institute of Space and Astronautical Science (ISAS) in Japan. CANOPUS data have been obtained with support of the Canadian Space Agency. We acknowledge the efforts of D. Wallis, who is responsible for the operations of the CANOPUS magnetometers. We thank the institutes who maintain the IMAGE magnetometer array and the Technical University of Braunschweig and the Finnish Meteorological for the use of the IMAGE data. The Greenland and PCN data were provided by Jurgen Watermann of Danish Meteorological Institute. Alaska chain magnetometer data were provided by John Olson of the Geophysical Institute of the University of Alaska. Energetic electron and ion fluxes from geosynchronous orbit satellites were provided by Geoffrey Reeves of Los Alamos of National Laboratory. Data from the stations in Russia were provided by K. Yumoto of Kyushu University. AE index was provided by World Data Center for Geomagnetism, Kyoto.

[32] Arthur Richmond thanks the reviewer for their assistance in evaluating this paper.

References

Angelopoulos, V. (1996), The role of impulsive particle acceleration in magnetotail circulation, in *Proceedings of the Third International Conference on Substorms* (*ICS-3*), *Spec. Publ. 389*, pp. 17–22, Eur. Space Agency, Noordwijk, Netherlands.

Angelopoulos, V., et al. (1993), Characteristics of ion flow in the quiet state of the inner plasma sheet, *Geophys. Res. Lett.*, *20*, 1711–1714.

Baumjohann, W., G. Paschmann, and H. Lühr (1990), Pressure balance between lobe and plasma sheet, *Geophys. Res. Lett.*, *17*, 45–48.

Erickson, G. M., and R. A. Wolf (1980), Is steady convection possible in the Earth's magnetotail?, *Geophys. Res. Lett.*, *7*, 897–900.

Fairfield, D. H. (1986), The magnetic field of the equatorial magnetotail from 10 to 40 R_E, *J. Geophys. Res.*, *91*, 4238–4244.

Fairfield, D. H., R. P. Lepping, E. W. Hones Jr., S. J. Bame, and J. R. Asbridge (1981), Simultaneous measurements of magnetotail dynamics by IMP spacecraft, *J. Geophys. Res.*, *86*, 1396–1414.

Fairfield, D. H., M. H. Acuna, L. J. Zanetti, and T. A. Potemra (1987), The magnetic field of the equatorial magnetotail: AMPTE/CCE observations at R < 8.8 R_E, *J. Geophys. Res.*, *92*, 7432–7442.

Fujimoto, M., T. Terasawa, and T. Mukai (1998), The low-latitude boundary layer in the tail-franks, in *New Perspectives on the Earth's Magnetotail*, *Geophys. Monogr. Ser.*, vol. 105, edited by A. Nishida, D. N. Baker, and S. W. H. Cowley, pp. 33–44, AGU, Washington, D. C.

Hori, T., K. Maezawa, Y. Saito, and T. Mukai (2000), Average profile of ion flow and convection electric field in the near-Earth plasma sheet, *Geophys. Res. Lett.*, *27*, 1623–1626.

Huang, C. Y., and L. A. Frank (1986), A statistical survey of the central plasma sheet: Implications for substorm models, *Geophys. Res. Lett.*, *13*, 652–655.

Huang, C. Y., and L. A. Frank (1994a), Magnitude of B_Z in the neutral sheet of the magnetotail, *J. Geophys. Res.*, *99*, 73–82.

Huang, C. Y., and L. A. Frank (1994b), A statistical survey of the central plasma sheet, *J. Geophys. Res.*, *99*, 83–95.

Katamura, C. (1997), *Near-Earth magnetospheric convection*, M. S. thesis, 23 pp., Univ. of Tokyo, Japan.

Kistler, L. M., E. Möbius, W. Baumjohann, G. Paschmann, and D. C. Hamilton (1992), Pressure changes in the plasma sheet during substorm injections, *J. Geophys. Res.*, *97*, 2973–2983.

Kistler, L. M., W. Baumjohann, T. Nagai, and E. Möbius (1993), Superposed epoch analysis of pressure and magnetic field configuration changes in the plasma sheet, *J. Geophys. Res.*, *98*, 9249–9258.

Kokubun, S., T. Yamamoto, M. H. Acuna, K. Hayashi, K. Shiokawa, and H. Kawano (1994), The Geotail magnetic field experiment, *J. Geomagn. Geoelectr.*, *46*, 7–21.

Mukai, T., S. Machida, Y. Saito, M. Hirahara, T. Terasawa, N. Kaya, T. Obara, M. Ejiri, and A. Nishida (1994), The low-energy particle (LEP) experiment onboard the Geotail satellite, *J. Geomagn. Geoelectr.*, *46*, 669–692.

Nagai, T., T. Mukai, T. Yamamoto, A. Nishida, and S. Kokubun (1997), Plasma sheet pressure changes during the substorm growth phase, *Geophys. Res. Lett.*, *24*, 963–966.

Nakamura, R., D. N. Baker, D. H. Fairfield, D. G. Mitchell, R. L. McPherron, and E. W. Hones Jr. (1994), Plasma flow and magnetic field characteristics near the midtail neutral sheet, *J. Geophys. Res.*, *99*, 23,591–23,601.

Spence, H. E., M. G. Kivelson, R. J. Walker, and D. J. McComas (1989), Magnetospheric plasma pressures in the midnight meridian: Observations from 2.5 to 35 R_E, *J. Geophys. Res.*, *94*, 5264–5272.

Terasawa, T., et al. (1997), Solar wind control of density and temperature in the near-Earth plasma sheet: WIND/Geotail collaboration, *Geophys. Res. Lett.*, *24*, 935–938.

Wang, C.-P., L. R. Lyons, M. W. Chen, and F. R. Toffoletto (2004), Modeling the transition of the inner plasma sheet from weak to enhanced convection, *J. Geophys. Res.*, *109*, A12202, doi:10.1029/2004JA010591.

Zhu, X. (1993), Magnetospheric convection pattern and its implications, *J. Geophys. Res.*, *98*, 21,291–21,296.

L. R. Lyons and C.-P. Wang, Department of Atmospheric and Oceanic Sciences, MS-7127, University of California, 405 Hilgard Avenue, Los Angeles, CA 90095-1565, USA. (larry@atmos.ucla.edu; cat@atmos.ucla.edu)

T. Nagai, Department of Earth and Planetary Sciences, Tokyo Institute of Technology, Ookayama 2-12-1 Meguro, Tokyo 152-8551, Japan. (nagai@geo.titech.ac.jp)

J. C. Samson, Department of Physics, University of Alberta, 412 Avadh Bhatia Physics Laboratory, Edmonton, Alberta, Canada T6G 2J1. (samson@space.ualberta.ca)